Holographic UV laser microsurgery

Aroshan K Jayasinghe,[1] Jason Rohner,[1] and M Shane Hutson[1,2,3,*]

[1]*Department of Physics & Astronomy, Vanderbilt University, Nashville, TN 37235, USA*
[2]*Department of Biological Sciences, Vanderbilt University, Nashville, TN 37235, USA*
[3]*Vanderbilt Institute for Integrative Biosystem Research & Education, Nashville, TN 37235, USA*
**shane.hutson@vanderbilt.edu*

Abstract: We use a spatial light modulator (SLM) to diffract a single UV laser pulse to ablate multiple points on a *Drosophila* embryo. This system dynamically generates a phase hologram for ablating a user-defined pattern fast enough to be used with living, and thus moving, tissue. We demonstrate the ability of this single-pulse multi-point system to perform two experiments that are very difficult for conventional microsurgery—isolating single cells *in vivo* and measuring fast retractions from large incisions.

OCIS codes: (070.6120) Spatial light modulators; (090.1995) Digital holography; (170.1020) Ablation of tissue

References and links

1. Y. Toyama, X. G. Peralta, A. R. Wells, D. P. Kiehart, and G. S. Edwards, "Apoptotic force and tissue dynamics during *Drosophila* embryogenesis," Science **321**(5896), 1683–1686 (2008).
2. M. S. Hutson, Y. Tokutake, M. S. Chang, J. W. Bloor, S. Venakides, D. P. Kiehart, and G. S. Edwards, "Forces for morphogenesis investigated with laser microsurgery and quantitative modeling," Science **300**(5616), 145–149 (2003).
3. X. Ma, H. E. Lynch, P. C. Scully, and M. S. Hutson, "Probing embryonic tissue mechanics with laser hole drilling," Phys. Biol. **6**(3), 036004 (2009).
4. D. P. Kiehart, C. G. Galbraith, K. A. Edwards, W. L. Rickoll, and R. A. Montague, "Multiple forces contribute to cell sheet morphogenesis for dorsal closure in *Drosophila*," J. Cell Biol. **149**(2), 471–490 (2000).
5. X. G. Peralta, Y. Toyama, M. S. Hutson, R. Montague, S. Venakides, D. P. Kiehart, and G. S. Edwards, "Upregulation of forces and morphogenic asymmetries in dorsal closure during *Drosophila* development," Biophys. J. **92**(7), 2583–2596 (2007).
6. E. R. Dufresne, G. C. Spalding, M. T. Dearing, S. A. Sheets, and D. G. Grier, "Computer-generated holographic optical tweezer arrays," Rev. Sci. Instrum. **72**(3), 1810 (2001).
7. E. R. Dufresne and D. G. Grier, "Optical tweezer arrays and optical substrates created with diffractive optics," Rev. Sci. Instrum. **69**(5), 1974 (1998).
8. J. Colombelli, E. G. Reynaud, and E. H. K. Stelzer, "Investigating relaxation processes in cells and developing organisms: from cell ablation to cytoskeleton nanosurgery," Methods Cell Biol. **82**, 267–291 (2007).
9. M. S. Hutson and X. Ma, "Plasma and cavitation dynamics during pulsed laser microsurgery *in vivo*," Phys. Rev. Lett. **99**(15), 158104 (2007).
10. A. Vogel and V. Venugopalan, "Mechanisms of pulsed laser ablation of biological tissues," Chem. Rev. **103**(2), 577–644 (2003).
11. V. Venugopalan, A. Guerra III, K. Nahen, and A. Vogel, "Role of laser-induced plasma formation in pulsed cellular microsurgery and micromanipulation," Phys. Rev. Lett. **88**(7), 078103 (2002).
12. A. Vogel, J. Noack, G. Hüttman, and G. Paltauf, "Mechanisms of femtosecond laser nanosurgery of cells and tissues," Appl. Phys. B **81**(8), 1015–1047 (2005).
13. K. Y. Lim, P. A. Quinto-Su, E. Klaseboer, B. C. Khoo, V. Venugopalan, and C.-D. Ohl, "Nonspherical laser-induced cavitation bubbles," Phys. Rev. E Stat. Nonlin. Soft Matter Phys. **81**(1), 016308 (2010).
14. P. A. Quinto-Su, V. Venugopalan, and C.-D. Ohl, "Generation of laser-induced cavitation bubbles with a digital hologram," Opt. Express **16**(23), 18964–18969 (2008).
15. A. Mao, "Holographic modulation of a pulsed UV laser microbeam for biophysical investigations of tissue dynamics," Senior Thesis (Free Electron Laser Laboratory, Duke University, 2004).
16. E. Fällman and O. Axner, "Design for fully steerable dual-trap optical tweezers," Appl. Opt. **36**(10), 2107–2113 (1997).
17. D. P. Kiehart, Y. Tokutake, M. S. Chang, M. S. Hutson, J. Wiemann, X. G. Peralta, Y. Toyama, A. R. Wells, A. Rodriguez, and G. S. Edwards, "Ultraviolet laser microbeam for dissection of *Drosophila* embryos," in *Cell Biology: A Laboratory Handbook*, 3rd ed., J. E. Celis, ed. (Elsevier Academic, 2006), pp. 87–103.
18. Y. Igasaki, F. Li, N. Yoshida, H. Toyoda, T. Inoue, N. Mukohzaka, Y. Kobayashi, and T. Hara, "High efficiency electrically-addressable phase-only spatial light modulator," Opt. Rev. **6**(4), 339–344 (1999).

#150309 - $15.00 USD Received 1 Jul 2011; revised 9 Aug 2011; accepted 9 Aug 2011; published 15 Aug 2011

19. E. Martín-Badosa, M. Montes-Usategui, A. Carnicer, J. Andilla, E. Pleguezuelos, and I. Juvells, "Design strategies for optimizing holographic optical tweezers set-ups," J. Opt. A, Pure Appl. Opt. **9**(8), S267–S277 (2007).
20. G. C. Spalding, J. Courtial, and R. Di Leonardo, "Holographic optical tweezers," in *Structured Light and Its Applications an Introduction to Phase-Structured Beams and Nanoscale Optical Forces*, D. Andrews, ed. (Academic Press, 2008), pp. 139–157.
21. R. Di Leonardo, F. Ianni, and G. Ruocco, "Computer generation of optimal holograms for optical trap arrays," Opt. Express **15**(4), 1913–1922 (2007).
22. M. Montes-Usategui, E. Pleguezuelos, J. Andilla, and E. Martín-Badosa, "Fast generation of holographic optical tweezers by random mask encoding of Fourier components," Opt. Express **14**(6), 2101–2107 (2006).
23. H. Oda and S. Tsukita, "Real-time imaging of cell-cell adherens junctions reveals that *Drosophila* mesoderm invagination begins with two phases of apical constriction of cells," J. Cell Sci. **114**(Pt 3), 493–501 (2001).
24. Lord Rayleigh, "On the pressure developed in a liquid during the collapse of a spherical cavity," Philos. Mag. **1917**, 34 (1917).
25. J. Campos-Ortega, *The Embryonic Development of Drosophila melanogaster*, 2nd ed. (Springer, 1997).
26. M. S. Hutson, J. Veldhuis, X. Ma, H. E. Lynch, P. G. Cranston, and G. W. Brodland, "Combining laser microsurgery and finite element modeling to assess cell-level epithelial mechanics," Biophys. J. **97**(12), 3075–3085 (2009).
27. J. Colombelli, E. G. Reynaud, J. Rietdorf, R. Pepperkok, and E. H. K. Stelzer, "*In vivo* selective cytoskeleton dynamics quantification in interphase cells induced by pulsed ultraviolet laser nanosurgery," Traffic **6**(12), 1093–1102 (2005).
28. J. Colombelli, S. W. Grill, and E. H. K. Stelzer, "Ultraviolet diffraction limited nanosurgery of live biological tissues," Rev. Sci. Instrum. **75**(2), 472 (2004).
29. J. Solon, A. Kaya-Copur, J. Colombelli, and D. Brunner, "Pulsed forces timed by a ratchet-like mechanism drive directed tissue movement during dorsal closure," Cell **137**(7), 1331–1342 (2009).
30. M. Rauzi, P. Verant, T. Lecuit, and P.-F. Lenne, "Nature and anisotropy of cortical forces orienting *Drosophila* tissue morphogenesis," Nat. Cell Biol. **10**(12), 1401–1410 (2008).
31. R. Farhadifar, J.-C. Röper, B. Aigouy, S. Eaton, and F. Jülicher, "The influence of cell mechanics, cell-cell interactions, and proliferation on epithelial packing," Curr. Biol. **17**(24), 2095–2104 (2007).
32. S. Kumar, I. Z. Maxwell, A. Heisterkamp, T. R. Polte, T. P. Lele, M. Salanga, E. Mazur, and D. E. Ingber, "Viscoelastic retraction of single living stress fibers and its impact on cell shape, cytoskeletal organization, and extracellular matrix mechanics," Biophys. J. **90**(10), 3762–3773 (2006).
33. I. Toytman, A. Silbergleit, D. Simanovski, and D. Palanker, "Multifocal laser surgery: cutting enhancement by hydrodynamic interactions between cavitation bubbles," Phys. Rev. E Stat. Nonlin. Soft Matter Phys. **82**(4), 046313 (2010).
34. Y. Tomita, A. Shima, and K. Sato, "Dynamic behavior of two-laser-induced bubbles in water," Appl. Phys. Lett. **57**(3), 234 (1990).
35. P. A. Quinto-Su and C.-D. Ohl, "Interaction between two laser-induced cavitation bubbles in a quasi-two-dimensional geometry," J. Fluid Mech. **633**, 425 (2009).

1. Introduction

Laser microsurgery is a well-established method for studying the cellular forces that drive morphogenesis [1–5]. In many cases, microsurgery creates extended incisions in a tissue by ablating discrete points one at a time—a serial multi-pulse procedure. Such incisions have proven useful in determining the relative morphogenetic roles of different tissue regions; however, the quantitative interpretation of such experiments is limited. Only the first pulse ablates unaltered tissue; all subsequent pulses ablate tissue that is already retracting or undergoing strain relaxation. This motion makes some potentially useful microsurgeries very challenging—*e.g.*, cutting around a single cell or patch of tissue to mechanically isolate it from a surrounding epithelium—and strongly interferes with the quantitative measurement of retraction velocity after extended incisions [1]. Here, we present a method for circumventing these problems by simultaneously ablating multiple points in a living tissue. We do so by dynamically shaping the phase profile of a single laser pulse using a programmable spatial light modulator (SLM).

SLMs are widely used to dynamically control multiple optical traps, a technique known as holographic optical tweezers [6,7]. The primary difference between an optical trapping setup and a microsurgical system is the use of a continuous-wave visible or near-IR laser in the former, but a pulsed laser in the latter. A wide variety of pulsed lasers have been used for laser microsurgery ranging from mode-locked near-IR systems running at 80 MHz to Q-switched UV systems running at only 10 Hz [8–12]. The choice of laser parameters for a given microsurgical application is driven by the scale of the targeted biological system (i.e. multi-cellular, cellular or sub-cellular), the acceptable level of collateral damage, and the time scales

#150309 - $15.00 USD Received 1 Jul 2011; revised 9 Aug 2011; accepted 9 Aug 2011; published 15 Aug 2011

of the tissue dynamics of interest. Nanosecond UV lasers excel at cutting cell edges using just a single pulse in experiments designed to measure the mechanical retraction of surrounding cells on time scales of milliseconds and longer. Such experiments could also be done using amplified femtosecond lasers, but less-expensive nanosecond UV lasers ablate with similarly low thresholds [9,12]. They have thus become the instrument of choice for microsurgical investigations of cellular mechanics. Here we show how nanosecond UV lasers can be coupled with an SLM to provide new and innovative means to probe cellular mechanics. Although pulsed lasers have been used in SLM-based ablation systems to study multi-point cavitation in liquids [13–15], pulsed UV exposure places unique demands on SLM damage thresholds for holographic microsurgery. In addition, the simultaneous ablation of multiple points may lead to unintended interactions between multiple cavitation bubbles in the tissue—confounding interpretations of the post-ablation tissue movements. We investigate both potential limitations below and find that holographic microsurgery must consider both, but is not strongly limited by either.

2. Materials and methods

2.1. Optical path

Our experimental layout contains three independently controlled optical paths for ablation, confocal fluorescence imaging and high-speed bright-field imaging (Fig. 1).

The ablation path transports light from the third harmonic of a Q-switched Nd:YAG laser (Minilite II, 4-ns pulse-width, $\lambda = 355$ nm, Continuum, Santa Clara, CA) to ablate tissue with either a steerable single-point [3,16,17] or a single-pulse, multi-point configuration using a programmable phase-only SLM (PPM X8267, Hamamatsu Photonics K.K., Japan) [18]. For single-point ablations, the SLM can be used as a mirror (76% reflectivity at 355 nm); however, using an overabundance of caution, we avoid such use of the SLM and instead place a mirror just in front of it to avoid unnecessary UV exposure. This replacement can be made with little loss of efficiency [19,20]. Lens pair L_1-L_2 expands the ablating beam to fully cover the SLM's 20 × 20-mm active area. Lens pair L_3-L_4 then projects the phase-modified beam onto the back aperture of a microscope objective (40×, 1.3 NA). A mask placed at the conjugate focus after L_3 removes unwanted diffractive orders. To summarize energy losses in the optical path, 76% of the energy incident on the SLM is reflected, less than 40% of which passes the mask (the first diffractive order contains less than 20% of the light, but the mask also passes higher positive diffractive orders), and only 40% of light passing the mask is transmitted through the optics and objective to the sample. Thus, the first-order pattern in the objective's focal plane contains less than 6% of the light incident on the SLM. The higher diffractive orders are individually weaker and below the threshold for ablation.

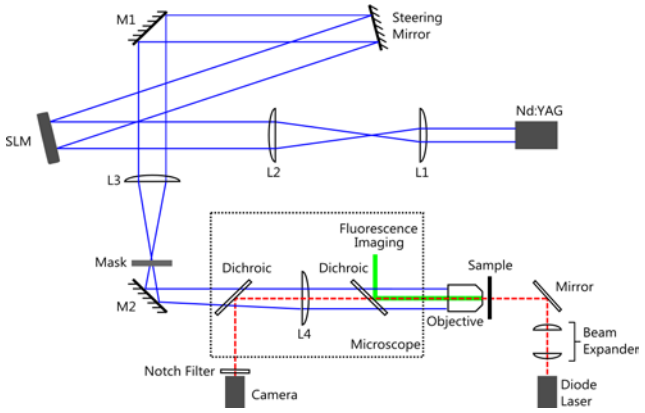

Fig. 1. Optical layout with paths for ablation, high-speed bright-field imaging and confocal fluorescence imaging shown in solid blue, dashed red and thick green lines, respectively.

#150309 - $15.00 USD Received 1 Jul 2011; revised 9 Aug 2011; accepted 9 Aug 2011; published 15 Aug 2011

Since exposure to a pulsed UV laser could damage the SLM, we evaluated damage thresholds by directing a 3-mm-diameter beam through a non-pixelated 25-mm-diameter SLM test cell—essentially a large 'single-pixel' device (Boulder Nonlinear Systems Inc., Lafayette, CO)—and evaluated damage as a loss of voltage-dependent birefringence. At a pulse repetition rate of 10 Hz, damage occurred for average intensity greater than 0.14 W/cm^2, which corresponds to peak intensity greater than 3.5 x 10^6 W/cm^2. To maintain a large safety margin, we only exposed the SLM to peak intensity <1.9 x 10^5 W/cm^2. With the current optical configuration, this corresponds to pulse energy <3 mJ. The average intensity threshold is of lesser concern because the SLM is exposed to less than ten ablation pulses and a few dozen lower energy alignment pulses in a typical five-hour experimental session. Within these safety margins, our microsurgery system is still capable of simultaneous ablation at over thirty points.

The fluorescence imaging path is used to track cell and tissue movements and is needed for precise targeting of the ablating laser to specific cells or tissue regions. This path is internal to an inverted laser-scanning confocal microscope (LSM 410/Axiovert 135TV, Carl Zeiss, Thornwood, NY). The high-speed bright-field imaging path is used to monitor the dynamics of ablation-induced cavitation bubbles (typically in a liquid sample instead of the highly-scattering tissues). The illumination source is a pulsed diode laser (Cube, λ = 660 nm, Coherent, Santa Clara, CA) and images are recorded by a high sensitivity CCD camera (CoolSNAP EZ, Photometrics, Tucson, AZ). A filter in front of the camera cuts out all light except for a narrow band around 660 nm. The strobe length of the pulsed diode laser (≥ 10 ns) and the delay between the ablation pulse and the laser strobe are both set using a digital delay generator (SRS DG645, Stanford Research Systems, Sunny Vale, CA). The imaging paths and ablating beam are co-aligned through dichroics to allow concurrent ablation and imaging.

2.2. Generating the phase hologram

To create a user-defined ablation pattern, we introduce a position-dependent phase onto the ablating beam's profile (using the phase-only SLM). The required phase hologram is calculated using a weighted Gerchberg-Saxton algorithm [21] that assumes a fixed amplitude profile in the phase plane and iteratively varies the phase hologram [20,22]. An initial guess for the appropriate phase hologram is generated by discretizing the desired ablation pattern (*e.g.*, a 10-μm line segment might be approximated by six points spaced 2-μm apart), calculating the 2D Fourier transform of each point independently, multiplying each transform by a different complex number or weight, summing all of the weighted transforms, and taking the spatially varying phase of this final sum. This initial guess is then used, together with the known optical characteristics of our system, to calculate the expected intensity distribution in the objective image plane. The uniformity of this distribution is used to calculate a new set of complex weights for the next iteration. This process is repeated until the calculated output converges on the target ablation pattern with sufficient uniformity. The weighting scheme prioritizes speed and uniformity over diffraction efficiency. As such, efficiency is low (<20%) and drops rapidly as the number of points increases. Given this drop in efficiency, the most complex pattern we have been able to ablate contains sixty points.

After convergence, the calculated phase hologram is written to the SLM as an 8-bit, 768 × 768-pixel image. The software for phase calculations and SLM control was developed and implemented using LabVIEW (National Instruments, Austin, TX) and Visual C++ (Microsoft, Redmond, WA).

The entire process—obtaining a confocal image of the sample, designing an ablation pattern, calculating the corresponding phase hologram, writing this pattern to the SLM, and finally performing the ablation—takes about two minutes. The actual time depends strongly on the number of points in the discretized target pattern. Using a 40× objective, the target pattern is limited to a 160 × 64-μm area by the magnification of the optical path and the distance between pixel centers in the SLM. This is sufficient for a wide range of incisions.

#150309 - $15.00 USD Received 1 Jul 2011; revised 9 Aug 2011; accepted 9 Aug 2011; published 15 Aug 2011

2.3. Sample preparation

All microsurgeries were performed on a transgenic strain of *Drosophila*, ubi-DE-Cad-GFP (*Drosophila* Genetic Resource Center, Kyoto, Japan), that ubiquitously expresses a GFP-cadherin fusion protein to label epithelial cell borders [23]. Fly embryos were incubated until mid-dorsal-closure stage, then prepared and mounted as described in [3]. Embryonic tissues were imaged and ablated close to the cells' apical surface. The ablations are carried out sufficiently above ablation threshold (2-5×) to ensure clean and complete incisions from a single pulse, despite small variations in sample preparation and tissue depth, as well as fluctuations in the ablating laser [3].

2.4. Cavitation bubbles

We can use high-speed images of cavitation bubbles to ensure that all the targeted points are above ablation threshold and there are no unintended ablation points introduced by the dynamically generated hologram. To image cavitation bubbles, the ablation laser was focused ~15 µm into a cuvette filled with an ethanol solution of laser dye (LD-390, 0.56 g/L, Exciton, Dayton OH). We measured the ablation threshold of this solution (264 nJ) to be similar to that of embryonic tissue (215 nJ), and significantly less (approximately 1%) than that of deionized water (29.1 µJ). Nonetheless, for a given above-threshold pulse energy, the bubble lifetimes are similar in all three samples (Fig. 2). The advantage of having a low threshold is twofold. Less energy is required when recreating equivalent patterns of bubbles, and any effects due a lack of uniformity in the output pattern will be easily seen.

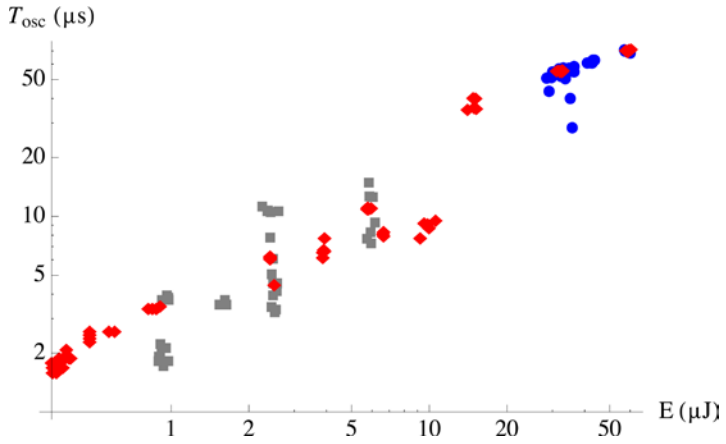

Fig. 2. Lifetime of laser-induced cavitation bubbles as a function of energy incident on the sample: red diamonds, solution of LD-390 in ethanol; gray squares, fruit fly embryos; blue circles, deionized water. Although the ablation thresholds differ by a factor of nearly 100, the bubble lifetime for a given pulse energy is consistent across all these samples.

To calculate ablation thresholds we placed a needle hydrophone (0.5 mm aperture, <20 ns rise time, 2.24 V/MPa sensitivity, Onda, Sunnyvale, CA) and recorded the pressure transients caused by the initial plasma and subsequent cavitation bubble collapse. The delay between these transients is a directly related to the bubble lifetime and can be used in the Rayleigh formula to approximate the maximum bubble radius [9,24].

3. Results and discussion

One challenging, but potentially useful microsurgery is to mechanically isolate a single epithelial cell *in vivo* (Figs. 3 and 4). The aim is to cut all of the cell-cell interfaces radiating away from a target cell, leaving that cell intact, but unconnected to the rest of the cell sheet. The isolated cell should relax to a size and shape dictated by intracellular forces.

Our target epithelium is the amnioserosa at Bowne's stage 14 [25] of fruit fly embryogenesis. Amnioserosa cells at this stage are approximately 10-20 µm in diameter and

#150309 - $15.00 USD Received 1 Jul 2011; revised 9 Aug 2011; accepted 9 Aug 2011; published 15 Aug 2011

3 µm thick with five to eight neighboring cells. Ablating a hole clean through one of the visible cell-cell interfaces releases the tensile stress both along that edge and across the apical surfaces of the adjoining cells [26]. Thus, five to eight cell edges need to be cut to isolate a single cell from the rest of the tissue.

With the conventional ablation system, a computer-controlled mirror steers the beam to cut cell edges one at a time (Fig. 3). This involves repeatedly taking confocal images of the tissue, targeting the moving edges and triggering the ablation laser. Each cycle takes tens of seconds, or longer if the tissue retracts strongly and one must wait to accurately target the next edge. During strong retraction, even an experienced operator will often miss a targeted edge, therefore requiring multiple ablations to cut some edges. During this drawn-out process, the cell-to-be-isolated may retract away from its original position and is often deformed by the anisotropic stresses present at intermediate stages. The order in which edges are targeted can usually minimize the retraction, but not the deformation. As a consequence, the size and shape of the isolated cell are not determined by intracellular forces, but are instead strongly influenced by the order and timing with which its connections to the rest of the sheet are severed. A high repetition rate laser, combined with a suitable scanning system can shorten the time required to cut a 30-µm diameter circle around a cell to just a few seconds [27,28], but this is still slow for use in applications that measure fast retractions on millisecond time scales [3].

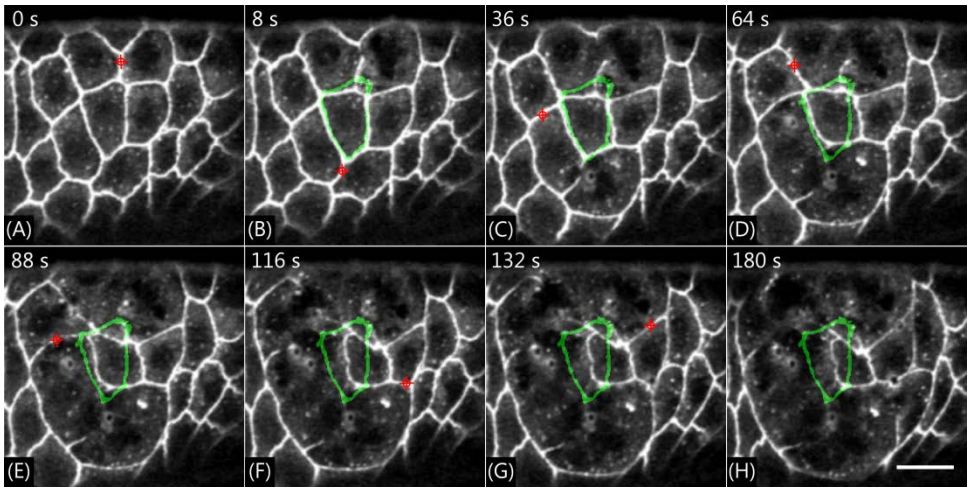

Fig. 3. Isolating a single cell from the amnioserosa using a conventional multi-pulse system (Media 1). The energy of each ablation pulse was 6.3 µJ at the mirror in front of the SLM—approximately 1.3 µJ at the sample, which is about 5× the ablation threshold. Each panel shows a confocal image of the tissue either (A) before or (B-H) during and after the sequence of ablations. Green overlays show the original outline of the cell to be isolated. Red crosshairs demarcate targets for the next ablation pulse. The static bright rings in the post-ablation images are holes in the embryo's overlying vitelline membrane. The 20-µm scale bar is common to all images. The time stamp for each panel is relative to the first image.

We then performed the same experiment using the single-pulse multi-point system (Fig. 4). To cut around a cell, we targeted the midpoints of all adjacent cell edges. Since the targeted cell edges may move during the iterative phase hologram calculation (at this stage of development, amnioserosa cells pulse with a period of about four minutes [29]), we targeted two closely spaced points per edge to maximize the probability of a clean and complete cut.

In the example shown, ten points are used to cut around the cell of interest, destroying six surrounding cells. The SLM-based multi-point ablation system is able to quickly and cleanly isolate a single large cell from the surrounding tissue with no visible damage to the isolated cell. Interestingly, although the surrounding tissue retracts strongly, the isolated cell initially shows only minor changes in shape, area and position (Figs. 4(B-C)) Only later, as the surrounding wound starts to heal, does the apical surface of the isolated cell autonomously

#150309 - $15.00 USD Received 1 Jul 2011; revised 9 Aug 2011; accepted 9 Aug 2011; published 15 Aug 2011

contract (Figs. 4(D-E)). We quantify these dynamics along a single line crossing the wound and isolated cell as shown in Fig. 4(F). The surrounding tissue initially retracts with a velocity of ~1.4 μm/s during the first four seconds, comparable to previous measurements in the amnioserosa [1,2,5,30,31] and slightly higher than the velocities seen for individually severed actin filaments in cultured endothelial cells [32]. Strain relaxation of this surrounding tissue occurs with a relaxation time of ~16 s and is complete by 50 s. In contrast, the apical surface of the isolated cell almost doesn't react to the ablation. Prior to ablation, it was expanding at a low rate of 30 nm/s; after ablation, it underwent a barely perceptible increase in expansion rate to 60 nm/s. Only after ~40 seconds does this isolated cell begin to contract at an average rate of 130 nm/s. Taken together, these results confirm that the tissue is under substantial tension; however, this tension places the cells under a very small elastic strain. Otherwise, the isolated cell would have immediately collapsed after ablation. On longer time scales, this isolated cell does undergo a sustained contraction, but the long pause implies that this is not a

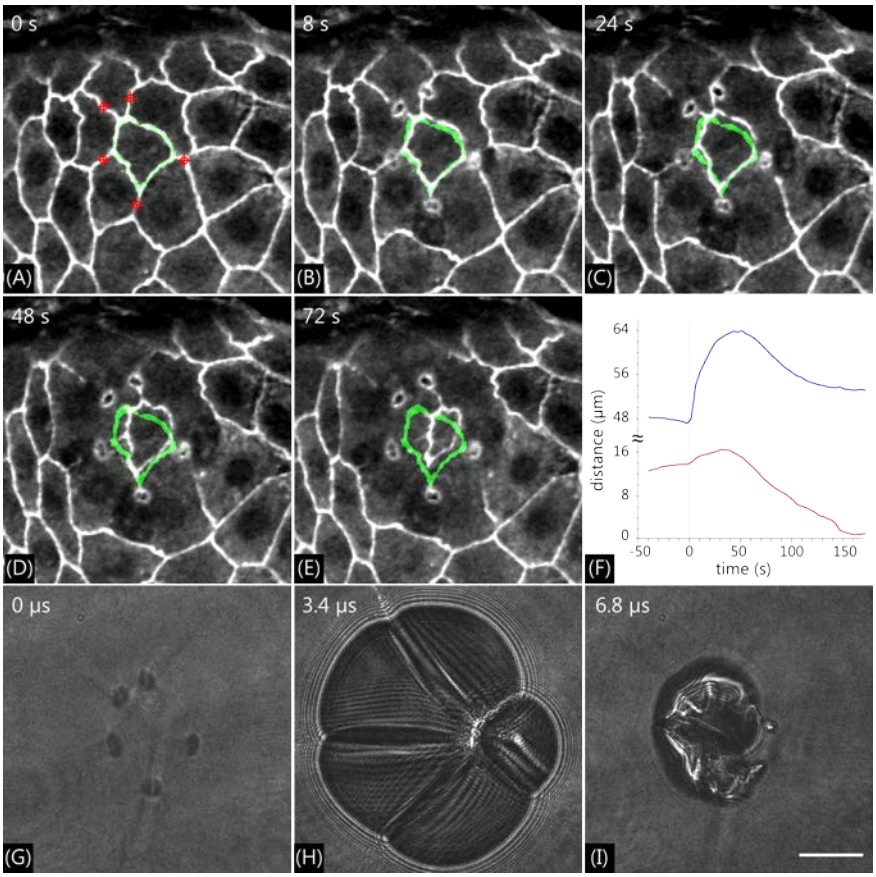

Fig. 4. Isolating a single cell from the amnioserosa using the single-pulse multi-point system (Media 2). The energy of the ablation pulse was 171 μJ at the surface of the SLM—approximately 10.3 μJ at the sample, which is about 4× the threshold expected for ten single-point ablations. (A) Confocal image of the tissue before ablation. Red crosshairs demarcate targets for ablation. (B-E) Confocal images after ablation. One can clearly see five holes in the overlying vitelline membrane. Green overlays show the original outline of the isolated cell. The time stamp for each panel is relative to the first image. (F) Comparison of the dynamic retraction of surrounding tissues (upper curve) and the collapse of the isolated cell (lower curve) as measured along a single line passing through the wound and isolated cell. (G-I) High-speed bright-field images of cavitation bubbles in solution. Images taken immediately post ablation, at maximum extent and at collapse with 10 ns exposures. Five pairs of cavitation bubbles can be seen in (G). The 20-μm scale bar is common to all images.

#150309 - $15.00 USD Received 1 Jul 2011; revised 9 Aug 2011; accepted 9 Aug 2011; published 15 Aug 2011

passive mechanical response. A thorough investigation of these biphasic dynamics and their implications for the mechanics of epithelial cells will be discussed elsewhere.

To assess the impact of cavitation bubbles on the ablated tissue, we used a hydrophone to measure the bubble lifetime *in vivo*. Using the same phase hologram and the same pulse energy on multiple embryos, we measured an average bubble lifetime of 6.9 µs. Using the Rayleigh relationship [24] for bubbles in water, this lifetime corresponds to a spherical bubble radius of 38 µm—surprisingly large given the limited damage evident in our confocal images. We could not directly image cavitation bubbles in the highly scattering *in vivo* environment, so we imaged lifetime-matched bubbles in a laser-dye solution (Figs. 4(G-I)). For matched lifetimes, spherical bubbles in this ethanol-based solution are predicted to be 6% larger than in water [24]. During the first 10 ns after the ablation pulse, one can clearly see five pairs of bubbles, corresponding to the five pairs of targeted ablation points (Fig. 4(G)). Importantly, even with some energy in higher diffractive orders, there are no unintended bubbles. The five pairs of bubbles expand over the next few microseconds to abut one another at their maximum extent. The individual bubbles are smaller than the Rayleigh prediction, but the agglomeration has a maximum extent (~80 µm) very close to twice this predicted radius. This extent clearly does not match the damage evident in our confocal images, suggesting that bubbles produced

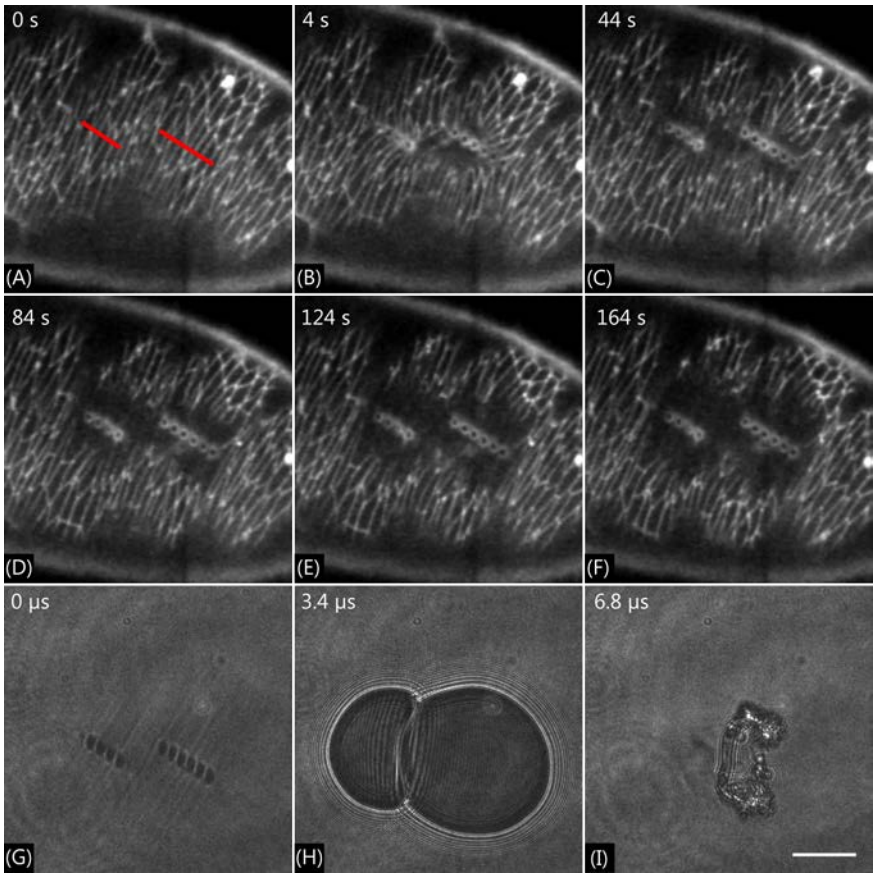

Fig. 5. Multi-point ablation for linear incisions in the lateral epidermis (Media 3). The energy of the ablation pulse was 146 µJ at the surface of the SLM—approximately 8.7 µJ at the sample, which is approximately 3× the threshold for ten single-point ablations. (A) Confocal image of the tissue before ablation. Red lines demarcate the targeted incisions. (B-F) Confocal images after ablation. (G-I) Lines of cavitation bubbles generated by same pattern in laser dye. Images was taken immediately post ablation, at maximum extent and at collapse with a 10 ns exposure. The common scale bar is 20-µm long.

#150309 - $15.00 USD Received 1 Jul 2011; revised 9 Aug 2011; accepted 9 Aug 2011; published 15 Aug 2011

in tissues do not behave the same as those in solution [33]. The *in vivo* bubbles may have a smaller extent for the same lifetime (due to elastic constraint by the surrounding tissue or to the fact that the environment of a fruit fly embryo is more nearly isochoric than isobaric) or may expand into the fluid trapped between the cell layer and the vitelline membrane that encases the embryo.

To further test the capabilities of the SLM-based system, we made linear incisions in the lateral epidermis of stage 14 fly embryos (Fig. 5). Each targeted incision was discretized with points spaced approximately 4 μm apart. This spacing was chosen to make a quasi-continuous cut in the epidermis (the cells of which are 3-4 μm across) while minimizing the total laser pulse energy. In Fig. 5, the shorter line is created by four ablation points, the longer by six.

In the confocal image immediately after ablation, one can see two lines of holes in the overlying vitelline membrane and some deformation of the epidermis (Fig. 5(B)). At later times, large holes in the epidermis open perpendicular to each linear incision (Figs. 5(C-F)). Using the same phase hologram and the same pulse energy on multiple embryos, we measured an average bubble lifetime of 6.8 μs. As before, this corresponds to a surprisingly large value for the predicted maximum bubble radius (37 μm) that is consistent with the maximum extent of matched-lifetime bubbles in laser-dye solution (~74 μm, Fig. 5(H)). Nonetheless, since the ablation process is complete within a few tens of microseconds, it is possible to measure a true initial retraction velocity and thus make solid inferences regarding variations in stress between adjacent segments of the epidermis. In a conventional laser microsurgery system, one must either compare incisions created in different embryos—thus conflating inter- and intra-embryo variations in tension—or compare sequential incisions in the same embryo—with the results dependent on the order of the incisions. The single-pulse multi-point ablation system eliminates both problems.

One new question that does arise with the multi-point ablation system is the possibility of hydrodynamic interactions between multiple cavitation bubbles [13]. Jets formed between closely-spaced bubbles could ensure complete ablation of the targeted edges in Fig. 4 and enhance the continuity of the linear incisions in Fig. 5 [33–35]; however, the bubbles in these patterns expand to such an extent that small scale jets are obscured by the large scale asymmetric collapse of the bubble agglomeration (Fig. 4(I) and Fig. 5(I)). Nevertheless, one should measure the hydrodynamic interactions for each class of ablation pattern and take those interactions into account when interpreting the mechanical implications of microsurgery in tissues.

4. Conclusions

Using a programmable, phase-only SLM, we can successfully ablate multiple points over a wide area (approximately 160 × 64 μm) with a single pulse from a nanosecond UV laser. We can dynamically generate the necessary phase hologram quickly enough to use this technique for microsurgical applications in living embryos. Care must be taken to measure and limit hydrodynamic interactions between simultaneous cavitation bubbles, but with proper care, this technique opens up several interesting research avenues including isolating single cells *in vivo* and measuring fast retraction from arbitrarily shaped wounds.

Acknowledgments

This work supported by the National Science Foundation (IOB-0545679) and the Human Frontier Science Program (RGP0021/2007C).

#150309 - $15.00 USD Received 1 Jul 2011; revised 9 Aug 2011; accepted 9 Aug 2011; published 15 Aug 2011